Accuracy assessment of high frequency radar current measurements in the Strait of Gibraltar

Pablo Lorente[1], Javier Soto-Navarro[1], Enrique Alvarez-Fanjul[1] and Silvia Piedracoba[2]

[1]Puertos del Estado, Madrid, Spain

[2]Departamento de Física Aplicada, Universidad de Vigo. Marcosende, Spain

Corresponding author:
Pablo Lorente
plorente@puertos.es

Abstract

An assessment of accuracy of a three site short-range (27 MHz) CODAR SeaSonde HF radar network deployed in the Strait of Gibraltar is attempted by comparing its surface current estimates with measurements from a moored point current meter. Radial and total current vectors are compared for a 47 day period from 19 October to 4 December 2013, yielding angular offsets, root mean square errors and correlations in the range 2º–30º, 8–22 $cm \cdot s^{-1}$ and 0.31–0.81, respectively. Statistics improve when the measured antenna pattern is used, except at one radar site. A self-consistency check in overwater baseline reveals that the dominant source of velocity differences is HF radar variance error.

1. Introduction

The Strait of Gibraltar constitutes a first order geostrategic spot as the only entrance gate to the Mediterranean Sea from the Atlantic Ocean (Fig 1a), with subsequent commercial concerns and a relevant trade volume related to the activity of the Port of the Bay of Algeciras (Fig 1b). Algeciras harbour operations include, among others - container transfer, bunker fuel handling, cruise shipping, layover and facilities for a fishing fleet. As a consequence, this region has one of the most intense maritime traffic levels in the world, becoming a vulnerable target for potential oil spill accidents - more than 100,000 ships cross it every year, transporting up to 20 million tonnes of fuel. Indeed, a number of harmful oil pollution episodes have been registered in recent years, like the *New Flame* (August 2007) or *Spabuinker IV* (January 2003).

A High Frequency (HF) radar was deployed in 2011 in order to monitor efficiently the surface current field in near real time, improving the operational oceanography infrastructure in the Strait of Gibraltar and enhancing a quick response to emergency situations.[1] This HF radar system has been installed within the framework of TRADE project (Trans-regional RADars for Environmental applications), as a result of a cooperative programme between Spain and Portugal (POCTEP), and has been supported by European FEDER funding.

Surface current measurements derived from HF radars have a broad range of practical applications[2] for Search and Rescue (SAR) operations,[3,4] oil spill transport models,[5] contaminant tracking or assimilation into numerical circulation models.[6,7,8]

As a preliminary step to the application of HF radar measurements, it is worthwhile to assess their reliability and accuracy and to evaluate intrinsic uncertainties. There are a variety of sources for uncertainties in HF radar estimations,[9] like radiowave interferences, antenna pattern distortions resulting from hardware problems, environmental noise or reflections due to dense sea traffic.[10,11] In this context, previous validation studies have been conducted with the aim of evaluating data uncertainties related to this technology through comparisons of total current vectors with current meter derived velocities.[12,13,14,15] Additionally, other investigations have focused on the estimation of errors in radial current vectors arising from individual radar sites[16,17,18,19,20,21] , since radial velocities and their associated uncertainties provide revealing information about data quality and site performance.[22]

The main goal of this paper is twofold. Firstly, to carry on and extend prior validation works achieved with the growing Spanish Coastal Ocean Radar Network, owned and operated by Puertos del Estado.[23,24] And secondly, to assess the accuracy of HF radar current measurements in such a key region as the Strait of Gibraltar represents, fostering the subsequent development of added-value operational tools.

According to this purpose, the present work builds on previous investigations,[18,20,21,25] devoted to the evaluation of direction-finding capabilities and the angular distribution of radial velocity uncertainties through the comparison of HF radar radial measurements with current estimations from single-point current meters and ADCPs. In this manuscript a similar analysis is presented, using data from three SeaSonde HF radar sites mounted around the Strait of Gibraltar (south of the Iberian Peninsula, Fig 1, a-b) and from a single-point current meter installed in a coastal buoy for a 47 day period from 19 October to 4 December 2013.

In addition, available overwater baselines are used for radar-to-radar comparisons. This internal consistency check provides the chance to explore quantitatively intrinsic uncertainties in radial current velocities. The influence of using ideal (not calibrated) or measured antenna patterns (hereafter referred to as IDEAL and MEAS, respectively) is examined for both radial measurements validation and radial selfconsistency test.

Furthermore, the present investigation is completed with an assessment of accuracy of total surface current vector maps. Zonal and meridional components of HF radar total current vectors (computed through the geometric combination of independent MEAS radial velocity measurements from the three radar sites), are compared with components of velocities estimated by the single-point current meter.

The paper is organised as follows, section 2 provides an oceanographic description of the study area. Section 3 outlines the specific instrumentation and methods used in this study. Section 4 presents a detailed discussion of the results and finally, a summary with concluding remarks is given in section 5.

2. Study area

The Strait of Gibraltar is a complex system of sills and narrows which extends across nearly 60km, with a mean width of 20km, connecting the Mediterranean Sea and the Atlantic Ocean. Its shallowest depth, of less than 300m, is found at Camarinal sill (CS) and the minimum width of around 14km is located at the Tarifa narrow (TN), both represented in Fig 1b. The freshwater deficit of the Mediterranean basin, a consequence of the excess of evaporation over precipitation and river runoff,[26,27,28] drives a two-layer baroclinic exchange in the Strait. A relatively fresh and warm Atlantic inflow of 0.81 ± 0.06 Sv (1 Sv = 106 m^3s^{-1}) enters the basin flowing eastward in the upper layer while a cooler and saltier Mediterranean outflow of −0.78 ± 0.05 Sv leaves the Strait flowing westward in the lower layer, resulting in a mean net flow of 0.038 ± 0.07 Sv.[2]

However, the exchange is not steady but highly variable at different time scales. Low frequency seasonal and interannual variability are mainly driven by the climatic forcing over the Mediterranean basin.[30,31] In the subinertial band (O (10 days)), the changes in the atmospheric pressure over the Western Mediterranean are the main mechanism affecting the flow, although the wind stress over the Atlantic side of the strait also plays a noticeable role. [32,33] By far, the most important sources of transport variability are the diurnal and semidiurnal tides, which cause the flow of the upper or lower layer at different points along the Strait to reverse in almost every tidal cycle. For instance, the tidal transport associated with M2 and S2 constituents reach values as high as 4 Sv.[34,35,36] Even though the meteorological wind forcing effect is restricted to the superficial layer, it might also be a key factor in specific processes such as punctual inflow interruptions or the circulation pattern in the Bay of Algeciras[37,38] (Fig 1b).

The HF radar system covers the easternmost area of the Strait of Gibraltar, including the mouth of the Bay of Algeciras and part of the western boundary of the Alboran Sea. The temporal coverage during the study period is higher than 80% in most of the domain, decreasing in the northeastern section (Fig 2b). The length of this period allows the analysis of short-term (subinertial to synoptic) variability. The mean velocity field provided by the system captures the main features of the area, i.e., the Atlantic Jet and a small portion of the Western Alboran Gyre (AJ and WAG, respectively, represented in Fig 1b), which generates a rather complicated circulation pattern in the area.[39]

As the HF radar velocity measurements are limited to the first meters of the water column, the wind-induced circulation, overlapping to the main flow, is the prevailing contribution to the velocity field. Fig 2a shows the 30h low-pass filtered[45] wind measured at a moored buoy situated within the HF radar domain (B1 in Fig 1b). The predominant wind directions are northeastern (NE) and southwestern (SW), as it can be deduced from the wind rose shown in Fig 2a. The circulation patterns induced by both components during especially intense and steady episodes are depicted in Fig 2, c-d, respectively. While NE winds overlap to the AJ, reinforcing the main current, SW winds generate a surface counter current, especially intense in the northeastern area. The results of Sánchez-Garrido[38] from high resolution model simulations show that these wind induced currents have a crucial role in the circulation pattern of the Bay of Algeciras, determining the flushing times at this highly sensitive area.

3. Instrumentation and methods

High Frequency Radar setup

HF radar stations measure ocean surface currents from the backscattered radar signal by surface gravity waves. This technology works on the principle of Bragg scattering where the transmitted electromagnetic radio pulses are reflected by resonant ocean surface waves of one-half the incident radar wavelength.[40] The difference between expected and observed Doppler shift is used to calculate the radial component of the surface current vector approaching to or receding from the station. Two or more radial vectors from independent stations are combined by a least squares method in order to calculate a total current vector. Extensive reviews of the basic functioning and operation of HF radars can be found in literature.[14,41]

The HF radar network employed in the present study consists of three shore-based 27 MHz short-range Seasonde sensors manufactured by Coastal Ocean Dynamics Applications Radar (CODAR) Ocean Sensors, Ltd, deployed in the Strait of Gibraltar, just in the western boundary of the Mediterranean Sea. The antennas, currently owned and operated by Puertos del Estado, were deployed in two stages. The first two antennas started data collection on May 2011: Ceuta (39.90ºN 5.31ºW) and Carnero (36.08ºN 5.43ºW). Afterwards, the third station Tarifa (36.00ºN 5.61ºW) was installed in October 2012 in order to resolve the baseline properly and to gain accuracy and insight over the entire radar coverage.

Hereafter the stations will be referred to by their four letter site codes: CEUT, CARN, and TARI, respectively (Fig 1b). Each site is operating at a central frequency of 26.8 MHz and providing radial measurements representative of current velocities in the upper 0.5 m of the water column. The maximum horizontal range is set to 40km, and the nominal range and angular resolutions are 1 km and 5º, respectively.

The radial velocities used in this study are based on hourly averaged backscatter data, and have been collected from 19 October to 4 December 2013. The current time series provided by the three stations present brief data gaps during the study period, (Fig 1c).

Buoy setup

The coverage area of the HF radar array includes one coastal ocean WatchKeeper buoy deployed since April 2009 in the southern waters of the Iberian Peninsula, moored in the northeastern boundary of the Strait of Gibraltar: Algeciras–Punta Carnero (36.07ºN, 5.42ºW, 40m depth), hereafter referred to as B1 (Fig 1b). This buoy is equipped with an ARG-SL single-point current meter (manufactured by Sontek) since August 2013, providing quality-controlled hourly averaged current velocity vectors at a nominal depth of 1m. Wind velocity measurements from B1 are used as a proxy for the local open sea wind conditions, and converted to neutral wind stress using the drag coefficient proposed in Large and Pound's[42] formulation, after correcting hourly data to 10m standard height.

It should be noted that B1 suffered from brief communication outages (Fig 1c) and subsequent gaps in data time series have been linearly interpolated.

Method 1: radial currents validation

Radial current time series produced during the 47-day study period by the three HF radar sites have been compared with radial current time series observed at B1 in order to assess the degree of agreement between both instruments and to evaluate sites performance in terms of bearing errors observed. This approach constitutes a useful tool for systematic quality data control and calibration of the HF radar system since results obtained using MEAS and IDEAL radial data are compared to infer the skill of direction-finding techniques.[43,44]

Hourly vector velocity time series from B1 have been projected onto the directions of each site. The component of moored current velocity in the radial direction has been calculated according to:

Equation (1): $r = U.\cos\alpha + V.\sin\alpha$

where *r* is the radial velocity in the direction of the radar site, α is the angle comprised between B1 and the radar site, and *U* and *V* are the east and north velocity components at B1 location, respectively.

In order to determine the bearing error, the range arc geographically closest to B1 has been selected for each of the HF radar sites (Fig 3a) and velocities estimated at each point of the arc have been compared with the radial projection of B1 velocities. By means of these comparisons, the evolution of several statistical parameters (root mean squared error and the correlation coefficient, hereafter referred as RMSE and R, respectively) along the selected arc have been calculated as a function of the angle comprised between B1 and the arc grid point position. In absence of direction-finding errors (DF), maximum R and minimum RMSE values should be found over the arc point closest to B1. In presence of DF, the bearing offset is thus expressed as:

Equation (2): $\Delta\alpha = \alpha_R - \alpha_M$

where α_R is the bearing to the arc point with maximum R and α_M is the bearing to the mooring buoy.

Furthermore, radial current time series have been filtered to remove any tidal effects or other high frequency components from the velocity data. Subinertial currents analysed in this paper have been resolved by applying a tenth order digital low-pass Butterworth filter with a cut-off period of 30h.[45]

The impact of using IDEAL or MEAS radials has been evaluated specifically for the expected best-match angle location by means of time series comparisons and best linear fit of the scatter plots of radar derived and observed radial currents.

Method 2: Baseline comparisons

Supplementary validation works with radial measurements have been carried out as the geometry of the emplacement gives the chance to analyse radar-to-radar overwater baselines in order to evaluate intrinsic velocity uncertainties in HF radial estimates.[20,22,46,47] This methodology states that, in the absence of errors, two facing sites should provide the same estimates of radial velocities (differing only in the sign) at the midpoint of the baseline that

joins them, since the range and the angular distribution are similar. This self-consistency test presents some benefits like the nonexistence of horizontal scale mismatch or depth mismatch, as the two involved sites are operating in the same frequency, providing two currents datasets with, in principle, identical origin and nature.

In the HF radar deployed in the Strait of Gibraltar, three different radar-to-radar baselines are available: TARI-CARN, TARI-CEUT and CARN-CEUT. The first one has been rejected from the analysis due to it being positioned over the coastline (Fig 3b**,** red dashed segment). The second one (orange dashed segment) has been also dismissed as CEUT site is oriented to the northeast and its range arcs do not reach the midpoint of the baseline defined between itself and TARI. Therefore, only CARN-CEUT (green dashed segment) has been analysed in the present consistency check. Hourly radial current time series from both sites have been compared at the midpoint (Fig 3b, red square), and the impact of using IDEAL or MEAS radial data has also been assessed.

Method 3: total currents validation

The main objective of this method is to assess the accuracy of total surface current vectors maps computed by means of combining independent calibrated (MEAS) radial velocity measurements from the three radar sites. Total current velocities profit because of having a smaller amount of gaps since vector computation takes advantage of radial velocities from several sectors surrounding the grid point.[18,25] On the contrary, the estimation of total vectors field introduces inherent errors which can possibly affect the quality of current data, quantified by the Geometric Dilution Of Precision (GDOP).[48,49] The GDOP is defined as a unit-less coefficient of uncertainty that characterises the effect of the geometry of the coupled radar system on the measurement and position determination errors.[50,51] Since B1 location is close to the baseline CARNCEUT, radial vectors arising from both sites will be nearly parallel at this place. Although the third radar site (TARI) properly resolves such baseline area contributing with nearly orthogonal radial vectors, the proximity to the coast of the line connecting TARI and B1 might lead to potential radiowave interferences and impact on the quality of radial vectors provided by TARI in B1 nearby regions. As a consequence, GDOP is expected to affect total current vectors accuracy[52] in the vicinity of B1 location.

A time series of hourly currents from the radar grid point closest to B1 location (called hereafter HFR1, positioned at 5.416ºW 36.067ºN) have been directly compared with current observations from B1 for the study period. Comparisons have been undertaken using zonal (U) and meridional (V) components in order to evaluate the agreement between both instruments' measurements by means of the computation of a set of statistical metrics - histograms, RMSE, scalar and complex correlations and best linear fit of scatter plots. Filtered time series obtained after applying a 30h low–pass Butterworth filter have been also compared to evaluate the discrepancies in subinertial currents. Additionally, complex correlations between near-surface B1 current data and nearby surface radar grid points have been calculated to explore the uniformity of the surface flow and to assess the directional error in radar-measured currents.

Finally, rotatory spectral analyses[53] have been performed for the HF radar surface total current vectors at HFR1 location and for current and wind stress data from B1 in order to identify the dominant modes of variability in the observations and the relationship between driving forces and surface current response. Since one specific

requirement for this kind of analysis is the continuity of the data record, small gaps encountered (not larger than 6h) in B1 time series have been linearly interpolated. Spectra have been calculated by dividing time series into successive six day segments, with a 50% overlap and a Hanning window[45], and subsequently averaged to provide some smoothing. Confidence levels for spectra densities have been derived assuming a chi-squared distribution for the variance.

4. Results

4.1 Radial currents validation

Bearing offset

Previous works established a typical magnitude for bearing error 5–20º,[18] with an angular offset of 10 to 15º for MEAS and up to 30º for IDEAL.[20] In the present work, bearing error (hereafter Δα) ranges between 2º and 30º, similar to prior reported values. Comparisons of radial currents estimated by B1 and CEUT (Fig 4, a-d), shows maximum correlation coefficients R in a grid point (denoted by vertical solid red line) angularly close to B1 location (vertical dotted black line): 0.49 for IDEAL and 0.45 for MEAS (statistically significant at 95% confidence level, with more than 1000 hourly observations), with associated Δα of 20º and 30º in the counterclockwise direction, respectively.

It should be noted that CEUT IDEAL seems to provide more accurate radial current estimations in the vicinity of B1 location since minimum RMSE are found there and associated R values are higher than those obtained with MEAS (0.43 versus 0.31, Table 1). Results derived from B1-CEUT filtered radial time series comparison reveal an enhancement of maximum R (0.84 for IDEAL and 0.81 for MEAS), a moderate reduction in RMSE (~27cm·s^{-1} and ~38cm·s^{-1}, respectively) and a relevant decrease of bearing offset value for MEAS (15º).

B1-CARN comparison reveals significantly better pairs of values R-RMSE: 0.74–18.51cm·s^{-1} for IDEAL and 0.74–15.63cm·s^{-1} for MEAS, with associated Δα values of 27º for both types of radials (Fig 4, e-f). The improvement detected for this site could be partially attributed to the fact that it is much closer to B1 than CEUT (range arc 2 versus arc 21) and the radiowave backscattered signal is stronger. Comparison of filtered radial time series gives evidence of an improvement in R-RMSE values (0.91–12.87cm·s^{-1} and 0.92–9.30cm·s^{-1} for IDEAL and MEAS, respectively) and also in the bearing error value for MEAS, decreasing to 22º (Fig 4h). According to these results, there is a clear improvement using MEAS, as also reflected in higher R found over B1 location (0.50 versus 0.43, Table 1).

Regarding B1-TARI comparison, results are poor so only outcomes from filtered time series are provided (Fig 4, i-j). The maximum R values are lower than previous ones (0.43) and angularly displaced 26º (2º) for IDEAL (MEAS). It should be noted an unsatisfactory representation of IDEAL radial currents in the vicinity of B1. Discrepancies could be explained by the influence of coupled factors such as the long distance between TARI and B1 (selected range arc is 19) and the proximity to the coastline of the line connecting both places, with subsequent potential radiowave

interferences. MEAS antenna pattern seems to solve, at least partially, these limitations since $\Delta\alpha$ is small and RMSE value is lower (23.94cm.s^{-1} versus 39.15cm.s^{-1}).

Time series of radial currents measured by B1 and those estimated in the closest range arc point ("best match-angle") by each HF radar site for the 47 day study period are presented in Fig 5. Time series exhibit sharp fluctuations mainly related to tidal variations, generally stronger in the case of HF radar sites measurements (solid red lines). Closer agreement between B1 (solid blue circles) and CEUT is found for IDEAL (Fig 5a), whereas MEAS leads to a better concordance between B1 and CARN and TARI sites (Figs 5d and 5f). Statistics derived from filtered time series comparison support this statement (Table 1). In addition, radar sites performance at the expected best-match angle is evaluated in terms of scatter plots of radar-estimated and observed radial currents. Best linear fit reveals slopes in the range [0.48, 0.83], with intercept values in the range (−8.97cm.s^{-1}; 10.10cm.s^{-1}) for CEUT and CARN, whereas values for TARI are statistically not significant (Table 1). Regression analyses of filtered time series show better results, with slope (intercept) closer to 1 (0) in the case of CEUT IDEAL, proving that it provides more accurate radial current measurements than MEAS. In contrast, MEAS seems to improve results for CARN and TARI.

Consistency check in the baseline

As previously mentioned, only CARN-CEUT overwater baseline fulfills the requirements to be examined thoroughly. The range arc points from both sites closest to the baseline midpoint are selected (Fig 3b) in order to compare their hourly radial velocities, obtained using IDEAL and MEAS antenna patterns. Results of the statistical baseline comparison are gathered in Table 1 (Section 2). The absolute value of the correlation R is slightly higher for MEAS (−0.55) than for IDEAL (−0.53). However, RMSE is noticeably lower for IDEAL (21.86cm.s^{-1} versus 38.22cm.s^{-1}, 40% smaller) and the best linear fit results are better, above all concerning the intercept value (which is closer to zero: −4.5cm.s^{-1} versus −26cm.s^{-1}) whereas slopes are quite similar (~ −0.35), indicating that the amplitude of velocity variations are up to 60% larger for CEUT than for CARN. These statements could be extrapolated to filtered time series, which shows a significant increase in absolute correlation values (up to −0.8) and a marked reduction in RMS differences, with decreases around 50%.

Previous works with overwater baselines[20,54,55] have reported slopes and intercepts in the ranges 0.58, 0.98 and −5, 4, respectively, with correlation coefficients above 0.5 and errors fluctuating from 5 to 13cm.s^{-1}. There are a variety of factors that could partially explain the differences observed and be responsible for lower than expected correlation values. On the one hand, whereas the predominant surface current flow in the Strait of Gibraltar is remarkably zonal, with prevalent eastern and northeastern directions,[38] the studied baseline presents a NW-SE orientation. This presumably could lead to less precise radial vectors in the baseline since radial measurements are proved to be more accurate when the dominant current flow moves in the same direction.[20,56] On the other hand, this region is characterised by highly variable flow exchanges[30,33] and by extremely intense current pulses,[57,58] reaching velocities up to 150 – 250cm.s^{-1}. These broad current speed ranges might put higher than reported RMSE values into the context of the observed variability.

With regards to the impact of using IDEAL or MEAS, the former seems to yield a better concordance between both datasets, considering the added fact that a higher amount of data is available for this antenna pattern (1092 versus 969, 11% higher). It could be attributed to the fact that CEUT measured antenna pattern significantly overestimates the radial currents velocities resolved by CARN, reinforcing the speculation (covered in previous section) that CEUT site is not properly calibrated or perhaps the measured antenna beam pattern was correct but has suffered from some quality degradation. Since MEAS should theoretically lead to more accurate radial current estimations (if the antenna pattern is done correctly[11]), hardware problems (related to strong winds, a typical feature in the Strait of Gibraltar) together with a troublesome maintenance, (in terms of logistic management as CEUT site is not deployed in the Iberian Peninsula but along the African shoreline) could likely explain higher error rates associated with MEAS.

Finally, the existence of a bearing offset in this site-to-site baseline comparison has not been investigated although it is expected, according to the results derived from previous section, that an angular shift might be present, as demonstrated in prior studies.[20,54] Future validation works could benefit from the recalibration of CEUT site and the widening of its radial coverage towards the western side in order to have the chance to analyse TARI-CEUT overwater baseline.

4.2 Total currents validation

Statistics derived from the comparison of zonal (U) and meridional (V) components of B1 and HFR1 for the 47-day analysed period are summarised in Table 2. It should be noted that the accuracy of HF radar-derived total current vectors will be affected by uncertainties related to MEAS radial vectors which are geometrically combined. In particular, inaccuracies observed in radial velocity measurements provided by the CEUT site will be propagated during the computation of surface total currents, impacting on their precision.

Differences in hourly current velocities for U and V are depicted in two histograms (Fig 6, a-b) which exhibit a quite symmetrical Gaussian-like shape, clustered around zero mean, slighlty shifted to negative (positive) values for the U (V) component, as indicated by the mean value –4.05 (2.93)cm.s^{-1}. Furthermore, histograms are not as tight as the range of zonal velocity differences presenting the same order of magnitude as the U velocity component for both instruments (standard deviation is 20.54cm.s^{-1} and mean velocities are 16.02 and 20.07cm.s^{-1} for B1 and HFR1, respectively), whereas meridional velocity differences are even one order of magnitude higher (standard deviation is 19.72cm.s^{-1} and mean velocities are 2.41 and –0.52cm.s^{-1} for B1 and HFR1, respectively).

Results gathered in Table 2 reveal a good agreement for U component, with a positive average flow W-E and a weak overestimation of mean zonal current velocities by the HF radar (20.07cm.s^{-1} versus 16.02cm.s^{-1}). In contrast, velocity differences observed for V are smaller in magnitude but more relevant in terms of direction since meridional mean value is positive for the point current meter (2.41cm.s^{-1}, northward) and negative for HFR1 (–0.52cm.s^{-1}, southward). Results derived from filtered time series comparison lead to similar conclusions, illustrated by a small decrease in velocity differences magnitude and its variability, with standard deviation ranging from 11 (V) to 12 (U)cm.s^{-1}.

With the objective of comparing the direction of the flow estimated by the two instruments, current roses have been depicted (not shown). The current meter registers a predominant flow towards the northeast (around 25º, assuming angles are measured counterclockwise from East), followed by a secondary main direction towards the southwest (−100º). However, HFR1 shows a wider variabilty, with a prevailing flow from West to East and current direction ranging from −25º to 25º. The histogram of direction differences (Fig 6c) between B1 and HFR1 current vectors shows a broad Gaussian-type shape, almost clustered around zero (mean and standard deviation values are −1.55º and 102.7º, repectively) and clearly shifted to positive values, which means B1 current vectors are predominantly shifted to the left of HFR1 currents. This mismatch is reduced for filtered time series (mean and standard deviation values are 1.21º and 61.43º, respectively).

Regression analysis (Table 2) reveals a slope of 0.59 between the U components measured by both instruments, where the intercept, correlation coefficient and RMSE are 11cm.s^{-1}, 0.61 and 20.93cm.s^{-1}, respectively. These results expose some HF radar performance features since they show a clear overestimation (subestimation) for small (high) values of zonal velocities. Regression slope and intercept for V component are 0.28 and −1.19cm.s^{-1}, respectively, and the associated correlation coefficient and RMSE are 0.45 and 19.93cm.s^{-1}. Complex correlation (CC) between B1 and HFR1 currents at zero lag is 0.57 with a phase of −15.67º between B1 and radar-derived measurements, indicating that the former are, on average, left shifted.

Results derived from filtered time series comparison remain rather constant for V whereas they improve significantly for U as the best linear fit parameters reach values of 0.98, 4.3 cm.s^{-1}, 0.77 and 12.8cm.s^{-1} for the slope regression, intercept, correlation coeficient and RMSE, respectively. CC also improves but moderately, exceeding 0.65 with an associated veering angle of −13.3º.

Spatial patterns of the complex correlation coefficient and its associated phase, together with scalar correlation and RMSE between B1-HFR1 zonal and meridional components are presented in Fig 7. All frequency bands are included in this analysis, which is mainly focused on the area surrounding B1 location (bold black square), not on the entire radar domain.

Complex correlations are moderately strong in the vicinity of B1, exceeding 0.55, and phases are about 15º (Fig 7, a-b). Correlation values present a quite uniform pattern in the zonal direction, decreasing more especially with distance in the alongshore direction. With regards to the orientation of current variability, the flow is rotated 20º to 30º clockwise relative to B1 data in the northern area, consistent with the shift to right of the mean flow (Fig 3b), whereas rather uniform orientation can be found in the southwestern area. Analysis also reveals that spatial distribution of zonal scalar correlation (Fig 7c) is nearly coincident with the pattern previously described for complex correlation, although values are slightly higher (above 0.6). Isolines of meridional scalar correlation are concentrically distributed around B1, with maximum values of 0.45 in nearby regions (Fig 7d). RMSE patterns exhibit a nearly-zonal distribution with lower values observed along the shore-line, in the range of 10–20cm.s^{-1} (Fig 7, e-f).

Spectral analyses have been computed to examine power spectral discrepancies in the frequency domain between both instruments. B1 and HFR1 current time series present qualitatively similar characteristics, capturing

properly the dominant features within the diurnal and semi-diurnal tidal bands (Fig 8, a-b). Significant non-polarised peaks are evident for both types of data (although their amplitude are slightly larger for B1 currents), related to prevalent rectilinear oscillation motions. Moderately good agreement between surface and sub-surface tidal variances is consistent with the mainly barotropic nature of the semidiurnal and diurnal tidal currents.[32,59] At the lower frequency synoptic time scales (< 0.4 cpd), differences between spectral energy levels can be observed since B1 spectrum indicates a subtle preference of clockwise (CW, solid red line, Fig 8a) rotating energies, while radar spectrum exhibits a counter-clockwise (CCW, solid blue line, Fig 8b) dominance with higher variance. A drop of energy and later flattening about 2.5 cpd are common for B1 and radar spectra. Finally, the wind stress spectrum is dominated by low-frequencies and shows non-polarised peaks at diurnal and semidiurnal frequencies (Fig 8c), although they are not so prominent and well-resolved as those observed in the previous spectra. The diurnal peak could be related to the influence of diurnal sea breeze.

5. Conclusions

An assessment of accuracy of a three site short-range (27 MHz) CODAR SeaSonde HF radar network deployed in the Strait of Gibraltar has been attempted by means of comparison with measurements from a moored point current meter installed in B1 buoy for a 47 day period from 19 October to 4 December 2013.

The comparison has been carried out at two different levels. The first level has consisted of the comparison of radar radial vectors from the closest range arc with the radial current component measured by B1. Observed bearing offsets range from 2º to 30º, similar to those reported in previous research.[18,20,25] Overall results indicate good correlations for radial velocities, with a general improvement for the calibrated antenna pattern (MEAS), except for CEUT site where IDEAL pattern leads to a higher agreement.

Discrepancies derived from TARI-B1 comparison could be attributed to the long distance between them together with the proximity to the shoreline of the line connecting both points. The geometry of the deployment provides the chance to carry out a self-consistency check in the over-water baseline joining CARN and CEUT. This test reinforces the hypothesis of an inadequate calibration of CEUT since more accurate values are obtained for IDEAL, although not as good as others reported in the literature.[20,54,55] Thus, according to the results (and leaving aside the fact that CEUT site is likely not properly calibrated), the dominant source of velocity differences between HF radar and B1 seems to be HF radar variance error. Additional sources of error that should be considered when validating HF radar data with in situ instruments are the mismatch in time sampling and averaging, different horizontal averaging scales, or contributions from Stokes drift likely included in HF radar-derived estimates.[60]

In the present study, mismatch in vertical scales does not play a significant role since HF radar (27 MHz) provides vertically integrated values representative of the upper 0.5m of the water column and the current meter gives measurements at 1m depth.

The second level has consisted in a comparison of HF radar total current vectors (constructed by means of the geometric combination of MEAS radial vectors from the three sites) and those measured by B1. Zonal component

of radar surface currents (U) tracked B1 subsurface component fairly well, consistent with previously reported values,[15,25] with a positive average flow W-E. However, meridional velocities (V) are only moderately well reproduced by the HF radar. There are a variety of limiting factors that might play a relevant role in reducing radar measurements accuracy, like the aforementioned differences between both instruments, or the B1 thorny location, moored near the shoreline, in the edge of HF radar coverage domain and rather close to CEUT-CARN baseline. Complementary validation works could benefit from the recalibration of CEUT site and the employment of drifters or ADCPs moored in strategic areas within HF radar domain, far from its boundaries and baselines.

Broadly speaking, the HF radar system deployed in the Strait of Gibraltar appears to properly represent basic oceanographic features and well-known mean circulation patterns observed and modeled in this area, according to maps depicted in Fig 2 b-d and prior results reported [38,39]. In this context, future works should include an extensive oceanographic description of the region, focusing especially on the scientific exploration of the Atlantic Jet, the assessment of primary meteorological forcing mechanisms and also a comprehensive tidal analysis since the most important sources of transport variability in the Strait of Gibraltar are the diurnal and semi-diurnal constituents. Other research lines could address the evaluation of circulation numerical models capabilities and the calibration-validation of operational ocean circulation systems currently running in this key region, like MyOcean IBI[61] or Sistema Autónomo de Medición, Predicción y Alerta en la Bahía de Algeciras (SAMPA[39]).

Acknowledgements

The authors gratefully acknowledge Qualitas Remos company (partner of CODAR) for their useful support and fruitful comments and suggestions.

References

1. Álvarez-Fanjul E, Losada I, Tintoré J, Menéndez J, Espino M, Parrilla G, Martínez I, and Muñuzuri VP. 2007. *The ESEOO Project: developments and perspectives for operational oceanography at Spain*. Proceedings, ISOPE2007: the 17th International Offshore Ocean and Polar Engineering Conference. Lisbon, Portugal. The International Society of Offshore Ocean and Polar Engineers (ISOPE), 3: 1708–1715.
2. Barrick DE, Evans MW and Weber BL. 1977. *Ocean surface currents mapped by radar*. Science, 198: 138–144.
3. Ullman D, O'Donnell J, Edwards C, Fake T, Morschauser D, Sprague M, Allen A and Krenzien B. 2003. *Use of coastal ocean dynamics application radar (CODAR) technology in US coast guard search and rescue planning.* US Coast Guard Technical Report, CG-D-09-03, 40.
4. O'Donnell J, Ullman D, Spaulding M, Howlett E, Fake T, Hall P, Tatsu I, Edwards C, Anderson E, McClay T, Kohut J, Allen A, Lester S and Lewandowski M. 2005. *Integration of Coastal Ocean Dynamics Application Radar (CODAR) and Short-Term Prediction System (STPS) surface current estimates into the search and rescue Optimal Planning System (SAROPS)*. US Coast Guard Technical Report, CG-D-01-2006.
5. Ullman DS, O'Donnell J, Kohut J, Fake T and Allen A. 2006. *Trajectory prediction using HF radar surface currents: Monte Carlo simulations of prediction uncertainties*. Journal of Geophysical Research, 111, C12005: 1–14.

6. Oke PR, Allen JS, Miller RN, Egbert GD and Kosro PM. 2002. *Assimilation of surface velocity data into a primitive equation coastal ocean model*. Journal of Geophysical Research, 107, C9, 3122: 1–25.
7. Paduan JD and Shulman I. 2004. *CODAR data assimilation in the Monterrey Bay area*. Journal of Geophysical Research, 109, C07S09, doi: 10.1029/2003JC001949.
8. Gopalakrishnan G and Blumberg AF. 2012. *Assimilation of HF radar-derived surface currents on tidal-timescales*. Journal of Operational Oceanography, 5, Nº 1: 75–87.
9. Lipa BJ. 2003. *Uncertainties in SeaSonde current velocities*. Proc. IEEE/OES Seventh Working Conference on Current Measurement Technology, San Diego, CA, IEEE/ OES: 1–6.
10. Kohut J, Roarty HJ and Glenn S. 2006. *Characterizing Observed Environmental variability with HF Doppler radar surface mappers and Acoustic Doppler Current Profilers: Environmental variability in the Coastal Ocean.* Journal of Oceanic Engineering, 31, Nº 4: 876–884.
11. Kohut JT and Glenn SM. 2003. *Improving HF radar surface current measurements with measured antenna beam patterns*. Journal of Atmospheric and Oceanic Technology, 20: 1303–1316.
12. Graber HC, Haus BK, Shay LK and Chapman RD. 1997. *HF radar comparisons with moored estimates of current speed and direction: Expected differences and implications*. Journal of Geophysical Research, 102, Nº C8, 18: 749–766.
13. Shay LK, Lentz SJ, Graber HC and Haus, BK. 1998. *Current structure variation detected by high frequency radar and vector measuring current meters*. Journal of Atmospheric and Oceanic Technology, 15: 237–256.
14. Paduan JD and Rosenfeld LK. 1996. *Remotely sensed surface currents in Monterey Bay from shore-based HF radar (CODAR)*. Journal of Geophysical Research, 101, 20: 669–686.
15. Kaplan DM, Largier J and Botsford LW. 2005. *HF radar observations of surface circulation off Bodega Bay (northern California, USA)*. Journal of Geophysical Research, 110, C10020: 1–25.
16. Laws KE, Fernandez DM and Paduan JD. 2000. *Simulation-based evaluations of HF radar ocean current algorithms*. IEEE Journal of Oceanic Engineering, 25: 481–491.
17. Laws K. 2001. *Measurements of near surface ocean currents using HF radar*. Ph.D. dissertation, Physics Department, University of California, Santa Cruz, CA.
18. Emery B, Washburn ML and Harlan JA. 2004. *Evaluating radial current measurements from CODAR highfrequency radars with moored current meters*. Journal of Atmospheric and Oceanic Technology, Vol. 21: 1259–1271.
19. Kim KC. 2004. *Calibration and validation of highfrequency radar ocean surface current mapping*. M.S. thesis, Oceanography Department, Naval Postgraduate School, Monterey, CA.
20. Paduan JD, Kim KC, Cook MS and Chávez FP. 2006. *Calibration and validation of direction-finding HighFrequency radar ocean surface current observations*. IEEE Journal of Oceanic Engineering, 31, Nº 4: 862–875.
21. Liu Y, Weisberg RH and Merz CR. 2010. *HF radar performance in a low-energy environment: CODAR SeaSonde Experience on the West Florida Shelf*. Journal of Atmospheric and Oceanic Technology, 27: 1689–1710.
22. Lipa B, Nyden B, Ullman DS and Terrill E. 2006. *SeaSonde radial velocities: derivation and internal consistency.* IEEE Journal of Oceanic Engeneering, 31 (4): 850–861.
23. Alfonso M, Álvarez-Fanjul E and López JD. 2006. *Comparison of CODAR SeaSonde HF Radar operational waves and currents measurements with Puertos del Estado buoys*. Final internal report of Puertos del Estado: 1–32.

24. Lorente P, Piedracoba S and Álvarez-Fanjul E. Submitted. *Calibration and Validation of High-Frequency Radar Ocean Surface Current Observations in the the NW of the Iberian Peninsula.* Continental Shelf Research.
25. Cosoli S, Mazzoldi A and Gacic M. 2010. *Validation of surface current measurements in the Northern Adriatic Sea from High Frequency radars*. Journal of Atmospheric and Oceanic Technology: 27–908.
26. Bethoux JP and Gentilli B. 1999. *Functioning of the Mediterranean Sea: Past and Present Changes related to freshwater input and climatic changes.* Journal of Marine Systems, 20: 33–47.
27. Mariotti A, Struglia MV, Zeng N and Lau KM. 2002. *The hydrological cycle in the Mediterranean region and implications for the water budget of the Mediterranean Sea*. Journal of Climate, 15: 1674–1690.
28. Criado-Aldeanueva F, Soto-Navarro J and GarcíaLafuente J. 2012. *Seasonal and interannual variability of surface heat and freshwater fluxes in the Mediterranean Sea: budgets and exchange through the Strait of Gibraltar*. International Journal of Climatology, 32: 286–302. doi:10.1002/joc.2268.
29. Soto-Navarro J, Criado-Aldeanueva F, GarcíaLafuente J and Sánchez-Román A. 2010. *Estimation of the Atlantic inflow through the Strait of Gibraltar from climatological and in situ data*. Journal of Geophysical Research, 115, C10023, doi:10.1029/2010JC006302.
30. García-Lafuente J, Delgado J, Vargas JM, Vargas M, Plaza F and Sarhan T. 2002a. *Low-frequency variability of the exchanged flows through the Strait of Gibraltar during CANIGO*. Deep Sea Research, II, 49: 4051– 4067.
31. García-Lafuente J, Delgado J, Sánchez-Román A, Soto J, Carracedo L and Díaz del Río G. 2009. *Interannual variability of the Mediterranean outflow observed in Espartel sill, western Strait of Gibraltar*. Journal of Geophysical Research, 114 C10, doi: 10.1029/2009JC005496.
32. Candela J, Winant CD and Bryden HL. 1989. *Meteorologically forced subinertial flows through the Strait of Gibraltar*. Journal of Geophysical Research, 94: 12667–12679.
33. García-Lafuente J, Álvarez-Fanjul E, Vargas JM and Ratsimandresy AW. 2002b. *Subinertial variability in the flow through the Strait of Gibraltar*. Journal of Geophysical Research, 107 (C10), 3168, doi:10.1029/ 2001JC001104.
34. García-Lafuente J, Vargas JM, Plaza F, Sarhan T, Candela J and Basheck B. 2000. *Tide at the eastern section of the Strait of Gibraltar*. Journal of Geophysical Research, 105: 14197–14213.
35. Bruno M, Mañanes R, Alonso JJ, Izquierdo A, Tejedor L and Kagan BA. 2000. *Vertical structure of the semidiurnal tidal currents at Camarinal Sill, the strait of Gibraltar.* Oceanologica Acta, 23: 15–24.
36. Sánchez-Román A, García-Lafuente J, Delgado J, Sánchez-Garrido JC and Naranjo C. 2012. *Spatial and temporal variability of tidal flow at the Strait of Gibraltar*. Journal of Marine Systems, 98–99: 9–17.
37. García-Lafuente J, Delgado J and Criado F. 2002c*. Inflow interruption by meteorologoical forcing in the Strait of Gibraltar.* Geophysical Research Letters, 29, 19, 1914.
38. Sánchez-Garrido JC, García-Lafuente J, Sammartino S, Naranjo C, de los Santos FJ and Álvarez-Fanjul E. 2014. *Meteorologically-driven circulation and flushing times of the Bay of Algeciras, Strait of Gibraltar*. Marine Pollution Bulletin, 80: 97–106.
39. Sánchez-Garrido JC, García-Lafuente J, ÁlvarezFanjul E, García Sotillo M and de los Santos F. 2013. *What does cause the collapse of the Western Alboran Gyre? Results of an operational ocean circulation system*. Progress in Oceanogrography, 116: 142–153

40. Paduan JD and Graber HC. 1997. *Introduction to highfrequency radar: Reality and myth*. Oceanography, 10: 36–39.
41. Prandle D. 1991. *A new view of near-shore dynamics based on observations from HF radar*. Progress in Oceanography, 27: 403–438.
42. Large WG and Pond S. 1981. *Open ocean momentum flux measurements in moderate to strong winds*. Journal of Physical Oceanography, 11: 324–366.
43. Barrick DE and Lipa BJ. 1986. *Correcting for distorted antenna patterns in CODAR ocean surface measurements*. IEEE Journal of Oceanic Engineering, OE-11: 304–309.
44. De Paolo T and Terrill EJ. 2007. *Skill assessment of resolving ocean surface current structure using compactantenna-style HF radar and the MUSIC direction-finding algorithm*. Journal of Atmospheric and Oceanic Technology, 24: 1277–1300.
45. Emery WJ and Thomson RE. 2001. *Data Analysis Methods in Physical Oceanography*. Elsevier Science, Amsterdam.
46. Atwater DP and Heron ML. 2010. *HF radar twostation baseline bisector comparisons of radial components*. Proceedings of Oceans 2010 IEEE Sydney. 24–27 May 2010, Sydney, NSW, Australia.
47. Laws KE, Vesecky JF and Paduan JD. 2011. *Error assessment of HF radar-based ocean current measurements: An error model based on sub-period measurement variance*. 01/2011; DOI:10.1109/CWTM.2011.5759527 ISBN: 978-1-4244-9285-5 In proceeding of: Current, Waves and Turbulence Measurements (CWTM), 2011 IEEE/OES 10th.
48. Chapman RD and Graber HC. 1997. *Validation of HF radar measurements*. Oceanography, 10, Nº 2: 76–79.
49. Ohlmann C, White P, Washburn L, Terril E, Emery B and Otero M. 2007. *Interpretation of coastal HF radarderived currents with high-resolution drifter data*. Journal of Atmospheric and Oceanic Technology, 24: 666–680.
50. Levanon N. 2000. *Lowest GDOP in 2-D scenarios*. IEEE Proceedings, Radar, Sonar Navigation, 147(3): 149–155.
51. Trujillo DA, Kelly FJ, Perez JC, Riddles HR and Bonner JS. 2004. *Accuracy of Surface Current Velocity Measurements Obtained from HF Radar in Corpus Christi Bay, Texas*. IEEE/ IGARSS Geoscience and Remote Sensing Symposium, 2: 1179–1182.
52. Barrick DE. 2002. *Geometrical Dilution of Statistical Accuracy (GDOSA) in Multi-Static HF Radar Networks*. CODAR internal document.
53. Gonella J. 1972. *A rotary-component method for analyzing meteorological and oceanographic vector time series*. Deep Sea Research, Part II, 19: 833– 846.
54. Cosoli S, Gacic M and Mazzoldi A. 2012. *Surface current variability and wind influence in the north eastern Adriatic Sea as observed from high-frequency (HF) radar measurements*. Continental Shelf Research, 33: 1–13.
55. Yoshikawa Y, Masuda A, Marubayashi K, Ishibashi M and Okuno A. 2006. *On the accuracy of HF radar measurement in the Tsushima strait*. Journal of Geophysical Research, 111, doi:10.1029/2005JC003232.
56. Robinson AM, Wyatt LR and Howarth MJ. 2011. *A two year comparison between HF radar and ADCP current measurements in Liverpool Bay*. Journal of Operational Oceanography, 4: 33–45.
57. Lacombe H and Richez C. 1982. *The regime of the Strait of Gibraltar.* In: Nihoul, J.C.J. (Ed.), Hydrodynamics of semi-enclosed seas. Elsevier Oceanography Series 34, New York: 13–73.

58. La Violette PE and Lacombe H. 1988. *Tidal-induced pulses in the flow through the Strait of Gibraltar*. Oceanológica Acta, SP9: 13–27.
59. Gomis D, Tsimplis MN, Martin-Miguez B, Ratsimandresy AW, Garcia-Lafuente J and Josey SA. 2006. *Mediterranean Sea Level and barotropic flow through the Strait of Gibraltar for the period 1958-2001 and reconstructed since 1659.* Journal of Geophysical Research, 111, C11005, doi:10.1029/2005JC003186.
60. Laws K, Paduan JD and Fernandez DM. 2003. *Effect of Stokes drift on HF radar measurements*. 1st International Workshop Radiowave Oceanography: 49–55.
61. Levier B, Cailleau S, Chanut G, Reffray G, Ayoub N, De Mey P, Lyard F, Maraldi C, Álvarez-Fanjul E and García-Sotillo M. 2010. *Development and assessment of the IBI operational ocean system*. MyOcean Science days. 1–2 December 2010, Toulouse, France.

542 TABLES

543

Section 1.- RADIALS COMPARISON RESULTS						
TIME SERIES (RAW)						
	CEUT		CARN		TARI	
	IDEAL	MEAST	IDEAL	MEAS	IDEAL	MEAS
N	1114	1057	1080	760		1078
R	0.43	0.31	0.43	0.50	1075 / −0.25	0.01
RMSE	18.11	37.32	15.48	19.63	85.55	53.87
TIME SERIES (FILTERED)						
	CEUT		CARN		TARI	
	IDEAL	MEAST	IDEAL	MEAS	IDEAL	MEAST
N	1114	1057	1080	760		1078
R	0.66	0.59	0.64	0.81	1075 / −0.18	0.17
RMSE	8.72	26.10	8.19	11.89	68.26	31.00
SCATTER PLOTS (RAW) HFR = A*BUOY+B						
	CEUT		CARN		TARI	
	IDEAL	MEAS	IDEAL	MEAS	IDEAL	MEAS
A	0.59±0.07	0.83±0.15	0.48±0.06	0.82±0.10	−0.41±0.09	0.01±0.09
B	1.90±1.07	10.10±2.30	1.48±0.89	−8.97±1.53	−61.20±2.94	−30.39±2.76

R2	0.19	0.10	0.18	0.25	0.06	0.00
SCATTER PLOTS (FILTERED) HFR = A*BUOY+B						
	CEUT		CARN		TARI	
	IDEAL	MEAS	IDEAL	MEAS	IDEAL	MEAS
A	1.01±0.07	2.12±0.17	0.54±0.04	1.63±0.08	−0.45±0.15	0.25±0.09
B	−0.37±0.61	3.25 ±1.63	1.94±0.42	−2.31±0.9	−61.16±2.17	−26.97±1.84
R2	0.44	0.35	0.41	0.66	0.03	0.03
Section 2.- RADIALS COMPARISON RESULTS IN BASELINES						
POINTS SELECTED						
	CARN		CEUT			
Arc	Longitude	Latitude	Arc	Longitude	Latitude	
11	5.369ºW	35.990ºN	11	5.367ºW	35.985ºN	
CARN - CEUT BASELINE COMPARISON RESULTS						
TIME SERIES						
	IDEAL (N = 1092)		MEAS (N = 969)			
	RAW	FILTERED	RAW	FILTERED		
R	−0.53	−0.79	−0.55	−0.80		
RMSE	21.86	11.75	38.22	20.20		
SCATTER PLOTS (CARN = A*CEUT +B)						
	IDEAL (N = 1092)		MEAS (N = 969)			

	RAW	FILTERED	RAW	FILTERED
A	−0.37 ± 0.02	−0.51 ± 0.01	−0.31 ± 0.02	−0.49 ± 0.01
B	−4.5 ± 0.53	−2.19 ± 0.27	−26.07 ± 0.85	−20.29 ± 0.58
R2	0.28	0.62	0.30	0.64

544 Table 1: (Section 1) Summary of results derived from radial current vectors comparison between B1 buoy and
545 the closest range arc point from three HF radar sites (CEUT, CARN, TARI) for the study period comprised from 19
546 October to 4 December 2013, using ideal and measured antenna patterns, for raw and 30h low-pass filtered time
547 series. (Section 2) Statistics derived from radar-to-radar comparison: radial current vectors self-consistency check at
548 the midpoint of the baseline that connects CARN and CEUT. N represents the number of hourly observations

TOTALS COMPARISON RESULTS (B1 -VS- HFR1) N = 1128								
	B1 Longitude		B1 Latitude		HFR1 Longitude		HFR1 Latitude	
	5.420ºW		36.070ºN		5.416 ºW		36.067ºN	
	TIME SERIES (RAW)				TIME SERIES (FILTERED)			
	U		V		U		V	
	B1	HFR1T	B1	HFR1T	B1	HFR1T	B1	HFR1T
MEAN	16.02	20.07	2.41	−0.52	15.95	19.97	2.24	−0.50
STD DV	23.74	22.96	21.67	13.52	14.80	18.94	12.28	7.41
R	0.61		0.45		0.77		0.47	
RMSE	20.93		19.93		12.80		11.30	
CC	0.57				0.68			
Veering	−15.67º				−13.30º			
	SCATTER PLOT (RAW)				SCATTER PLOT (FILTERED)			
	U		V		U		V	

A	0.59 ± 0.02	0.28 ± 0.03	0.98 ± 0.03	0.28 ± 0.02
B	11 ± 0.64	−1.19 ± 0.36	4.35 ± 0.52	−1.13 ± 0.19
HISTOGRAMS (DIFF B1-HFR1)				
DIFF	(RAW)		(FILTERED)	
U	−4.05 ± 20.54		−3.99 ± 12.18	
V	2.93 ± 19.72		2.74 ± 10.99	
θ	−1.55º ± 102.70º		1.21º ± 61.43º	

Table 2: Summary of results derived from total current vectors comparison between B1 buoy and the closest HF radar grid point (HFR1) for the study period comprised from 19 October to 4 December 2013, for raw and 30h low-pass filtered time series. Comparisons undertaken using zonal (U) and meridional (V) current components. N represents the number of hourly observations.

FIGURES

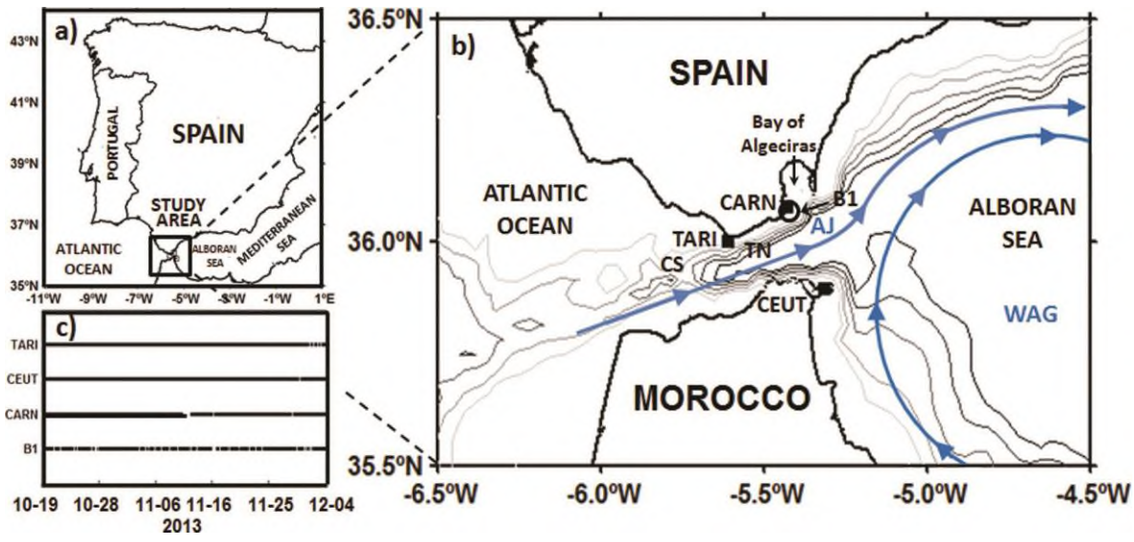

Fig 1: (a) General area of study. (b) Map of the Strait of Gibraltar. Locations of B1 buoy (circle) and three HF radar sites (filled squares): CEUT, CARN and TARI. Isobath depths (not labeled for clarity) are 100m, 200m, 300m, 400m, 500m and 600m. The topographic features shown are Camarinal Sill (CS) and Tarifa Narrows (TN). Blue contours represent stream lines: The Atlantic Jet (AJ) and the Western Alboran Gyre (WAG). (c) Time lines of HF radar sites and B1 current data availability for the 47 day study period.

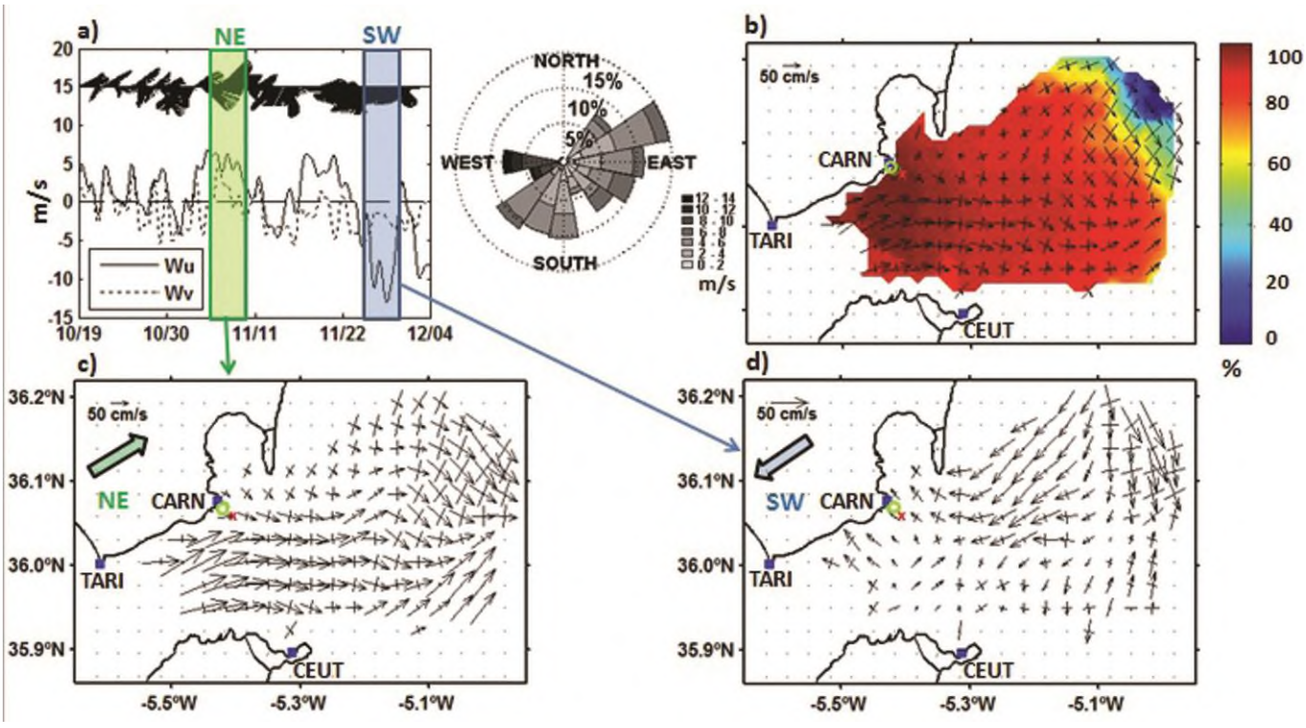

577

578 Fig 2: (a) 30h low-pass filtered zonal (Wu) and meridional (Wv) wind components measured by B1 buoy for the
579 study period comprised from 19 October to 4 December 2013. Wind rose shows predominant directions. (b)
580 Averaged total current vectors map. Cross bars indicate standard deviation (only one grid point of every three is
581 plotted for visualisation reasons). Contour colours denote the coverage percentage of total current vectors. Green
582 circle and red cross represent B1 and the closest HF radar grid point (HFR1) locations, respectively. (c) Five day
583 average HF radar surface currents during predominant northeastern (NE) wind field (5 to 9 November 2013). (d)
584 Five day average HF radar surface currents during predominant southwestern (SE) wind field (26 to 30 November
585 2013). The averaging times are denoted in the shaded upper panels depicted in (a)

586

587

588

589

590

591

592

593

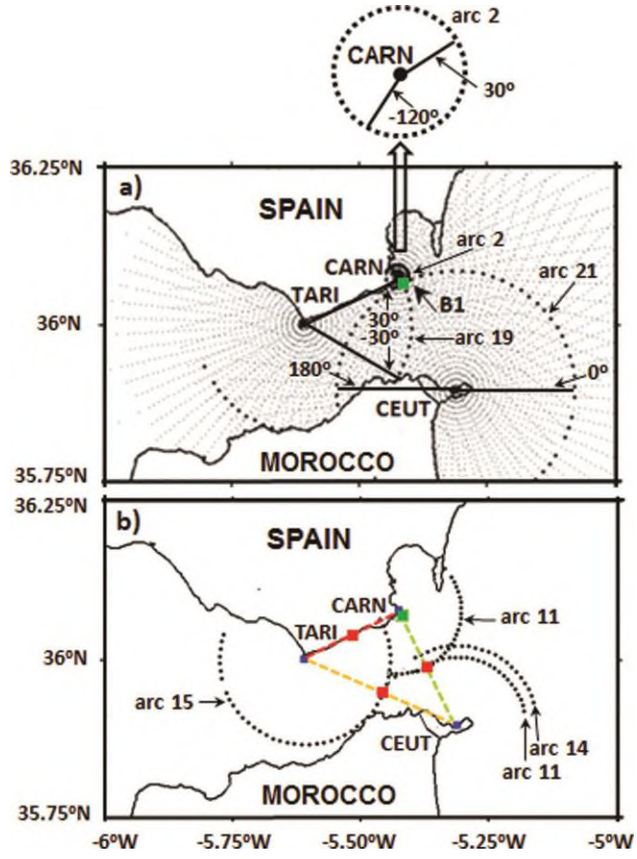

Fig 3: (a) Radial range arcs emerging from each HF radar site: CARN, CEUT and TARI. Bold black dots represent the range arcs selected (labeled according to their relative position respect the site they emerge from: far arcs have labels with higher values) to carry out radial current comparisons, closest to B1 buoy location (denoted by a solid green square). Angle values are measured counterclockwise from East and indicate arc limits. (b) Available baselines (colored dashed lines). Solid red squares denote the midpoint of each baseline where radar-to-radar comparison is performed. Only CARN-CEUT overwater baseline (green dashed line) is analysed since the rest do not fulfill the specific requirements. Bold black dots represent again the selected range arcs, closest to baseline midpoints (and labeled according to their relative location).

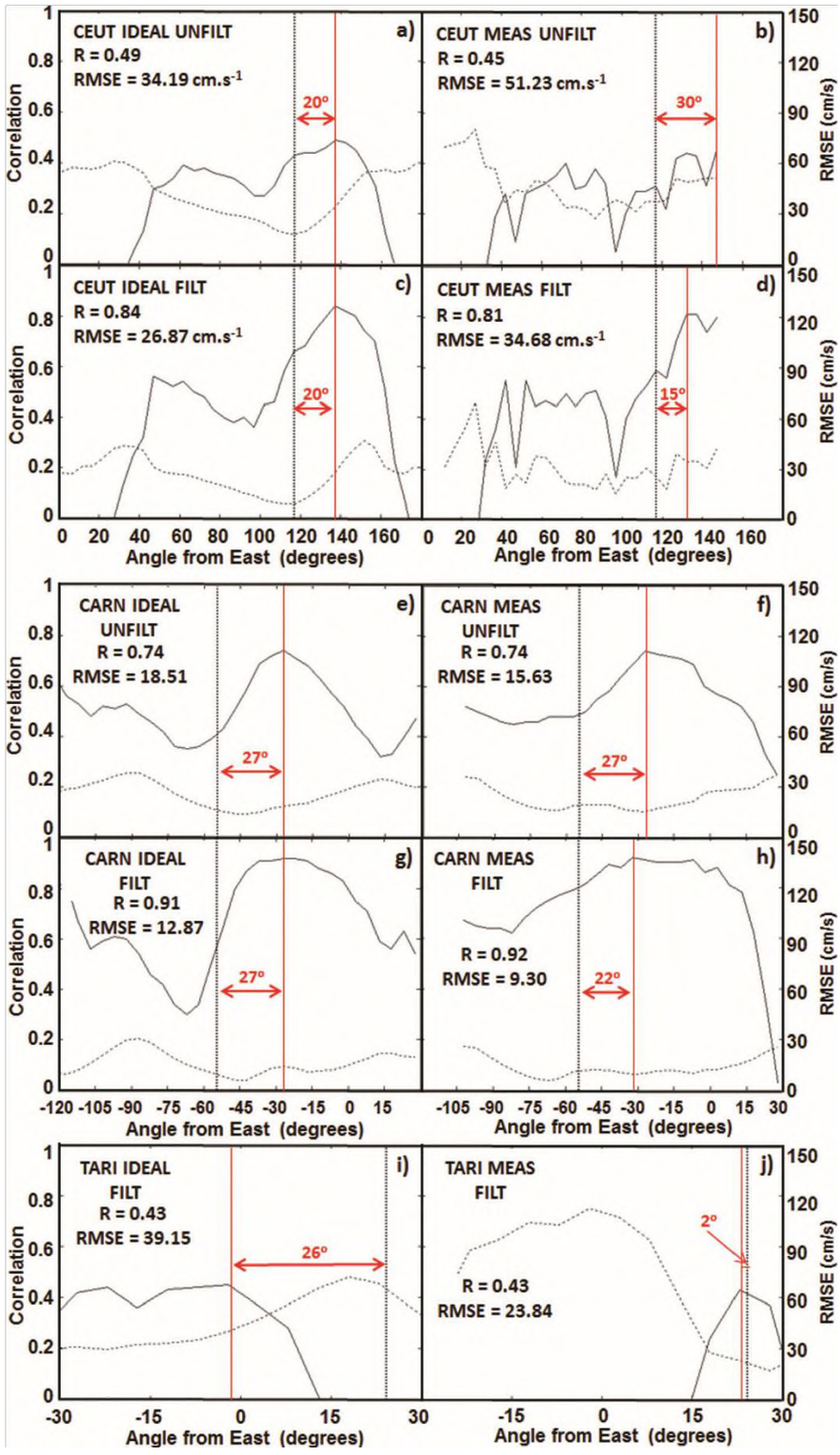

615 Fig 4: (a-j) Correlation (solid black line) and RMSE (dashed black line) between radial currents estimated by B1
616 buoy and three HF radar sites, CEUT (a-d), CARN (e-h) and TARI (i-j), using ideal (left panels) and measured (right
617 panels) antenna patterns, for the study period comprised from 19 October to 4 December 2013. For CEUT and CARN,
618 upper (lower) panels show results obtained for raw (30h low–pass filtered) time series. For TARI only results derived
619 from filtered time series are exposed. Vertical dotted black line represents the angular position of the B1 (angles
620 measured counterclockwise from East). Vertical solid red line denotes the angular position of maximum correlation
621 (R), which is gathered with the associated RMSE value.

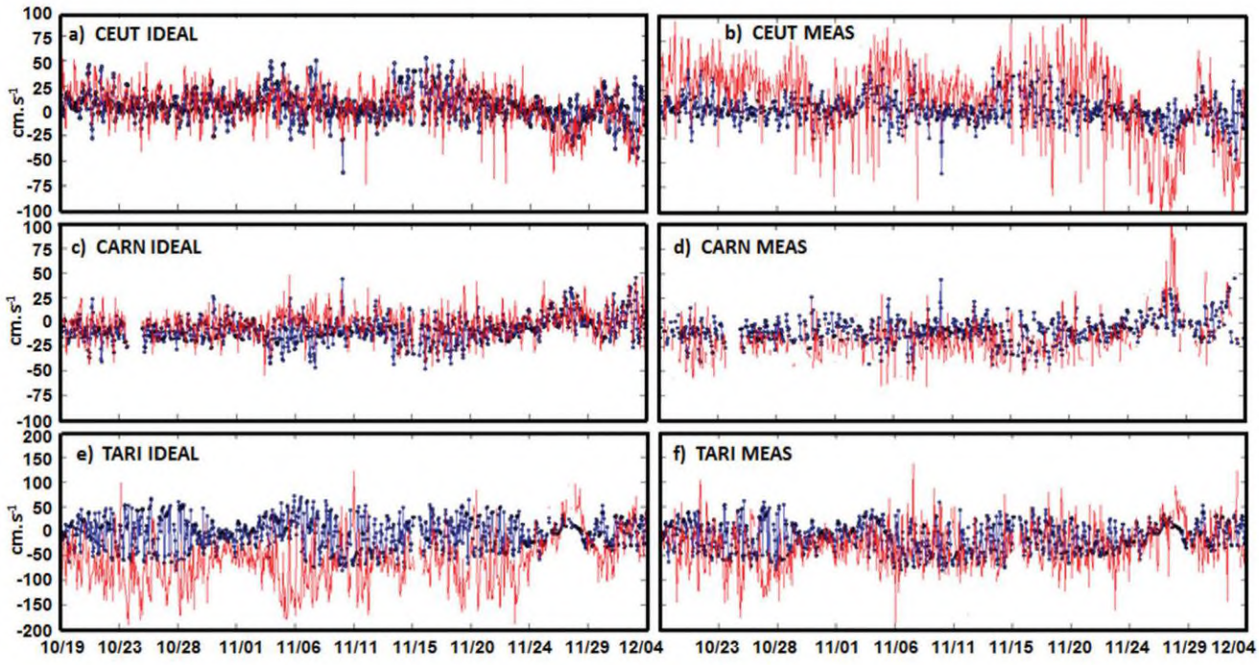

622

623 Fig 5: Time series of radial currents measured by B1 buoy (solid blue circles) and HF radar
624 sites (CEUT, CARN and TARI, red lines) in the range arc point closest to B1 location, using
625 ideal (left) and measured (right) antenna pattern.

626

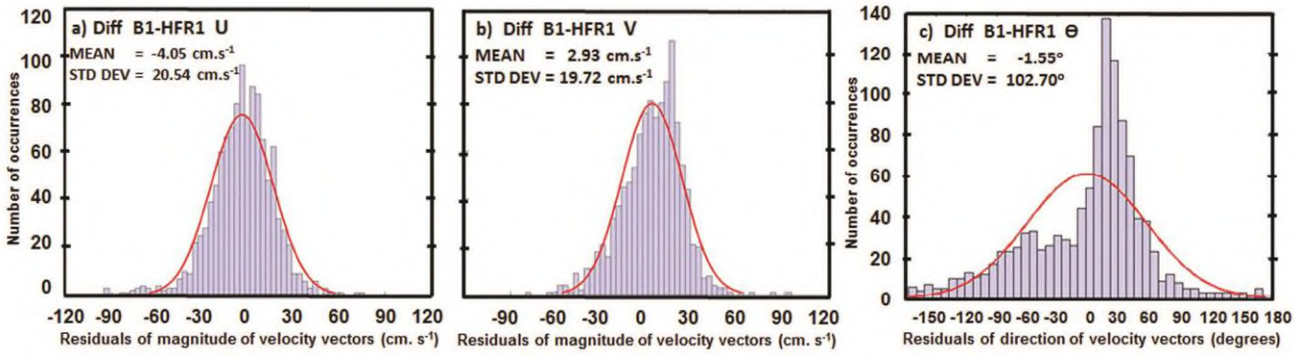

627

628 Fig 6: Histograms of current velocity differences between B1 buoy measurements and estimates from the closest HF
629 radar grid point (HFR1), for the (a) zonal and (b) meridional component. (c) Histogram of current vector directions
630 differences between B1 and HFR1. The red curve line represents a superimposed fitted normal density function.

631

632

633

634

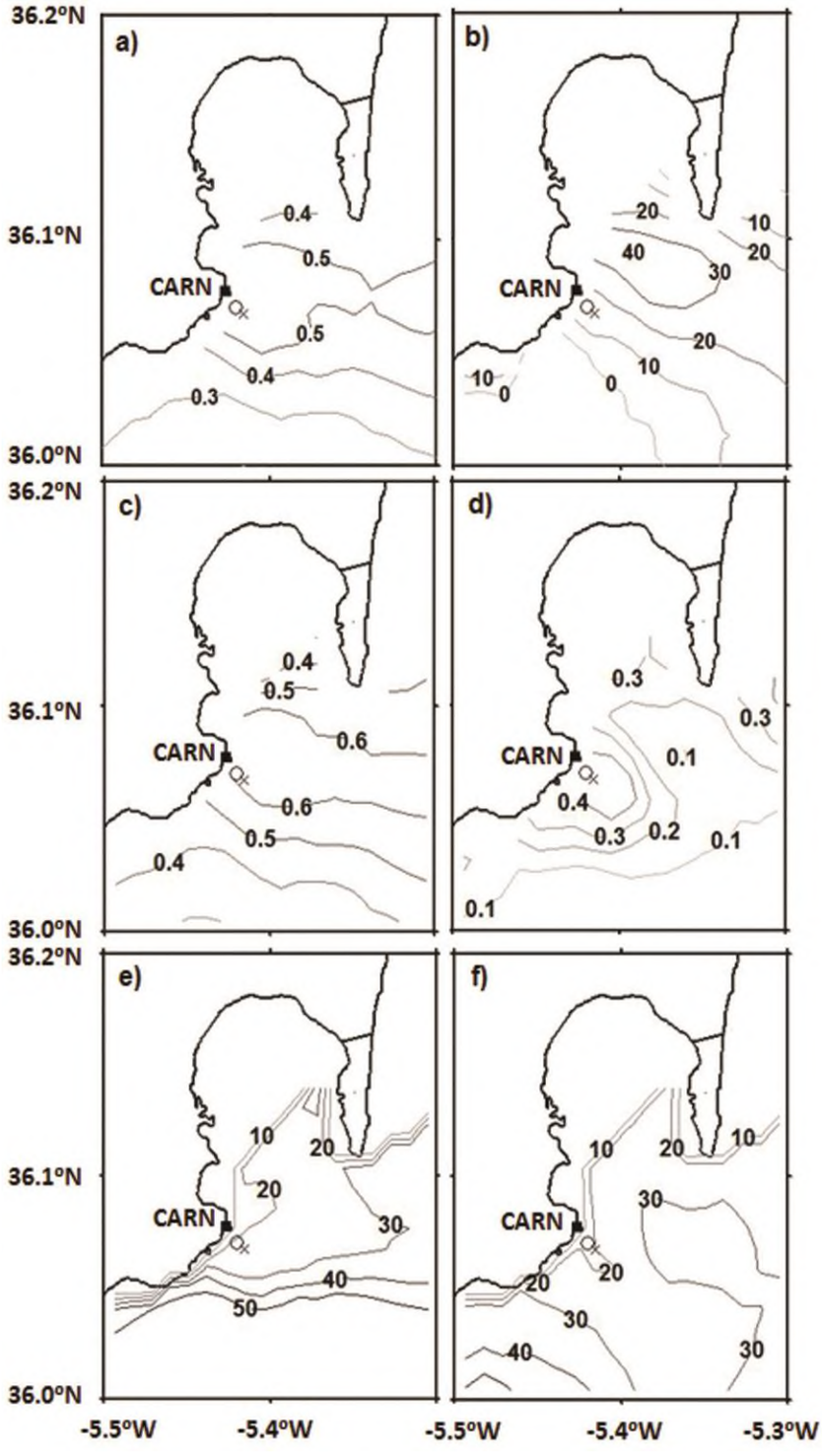

Fig 7: (a,b) Magnitude and phase (in degrees) of complex correlations between HF radar and B1 buoy (bold black circle) current data. Only radar grid points in the vicinity of B1 have been considered. Positive phase values mean that HF radar total current vectors are rotated clockwise relative to B1 current vectors. (c,d) Spatial distribution of the scalar correlation coefficient between HF radar and B1 current components: zonal (left) and meridional (right). (e,f) RMSE contour plots for the HF radar – B1 current components: zonal (left) and meridional (right). Data from all frequencies have been used in these comparisons. The bold red cross denotes the HF radar grid point closest to B1 location (called HFR1)

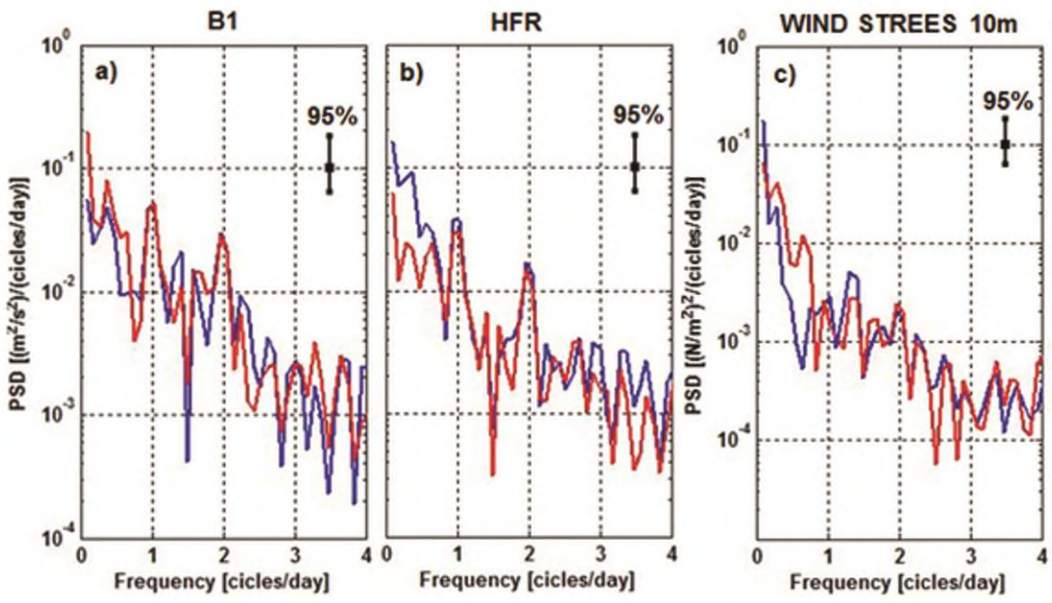

643

644 Fig 8: Power spectral densities of (a) B1 buoy, (b) HF radar at the closest grid point (HFR1) and (c) wind stress at
645 10m height derived from B1 wind measurements. Solid blue (red) lines represent the clockwise (counter-clockwise)
646 rotating component. Error bars indicate 95% confidence interval.